A distributed stream temperature model using high resolution temperature observations

M. C. Westhoff, H. H. G. Savenije, W. M. J . Luxemburg, G. S. Stelling, N. C. van de Giesen, J. S. Selker, L. Pfister, S. Uhlenbrook

Hydrol. Earth Syst. Sci. Discuss., 4, 125–149, 2007
www.hydrol-earth-syst-sci-discuss.net/4/125/2007/

Hydrology and Earth System Sciences Discussions

Papers published in *Hydrology and Earth System Sciences Discussions* are under open-access review for the journal *Hydrology and Earth System Sciences*

A distributed stream temperature model using high resolution temperature observations

M. C. Westhoff[1], H. H. G. Savenije[1], W. M. J . Luxemburg[1], G. S. Stelling[2], N. C. van de Giesen[1], J. S. Selker[3], L. Pfister[4], and S. Uhlenbrook[5]

[1]Water Resources Section, Faculty of Civil Engineering and Geosciences, Delft University of Technology, P.O. Box 5048, 2600 GA Delft, The Netherlands
[2]Fluid Mechanics Section, Faculty of Civil Engineering and Geosciences, Delft University of Technology, P.O. Box 5048, 2600 GA Delft, The Netherlands
[3]Department of Biological and Ecological Engineering, Oregon State University,116 Gilmore Hall, Corvallis, OR 97331, USA
[4]Department Environment and Agro-biotechnologies, Centre de Recherche Public – Gabriel Lippmann, 41, rue du Brill, 4422 Belvaux, Luxembourg
[5]Department of Water Engineering, UNESCO-IHE, Westvest 7, 2611 AX Delft, The Netherlands

Received: 18 December 2006 – Accepted: 22 January 2007 – Published: 26 January 2007

Correspondence to: M. C. Westhoff (m.c.westhoff@tudelft.nl)

Abstract

Highly distributed temperature data are used as input and as calibration data for a temperature model of a first order stream in Luxembourg. A DTS (Distributed Temperature Sensing) fiber optic cable with a length of 1500 m is used to measure stream water temperature with a spatial resolution of 0.5 m and a temporal resolution of 2 min. With the observations four groundwater inflows are found and quantified (both temperature and relative discharge). They are used as input for the distributed temperature model presented here. The model calculates the total energy balance including solar radiation (with shading effects), longwave radiation, latent heat, sensible heat and river bed conduction. The simulated temperature along the whole stream is compared with the measured temperature at all points along the stream. It shows that proper knowledge of the lateral inflow is crucial to simulate the temperature distribution along the stream, and, the other way around stream temperature can be used successfully to identify runoff components. The DTS fiber optic is an excellent tool to provide this knowledge.

1 Introduction

Rainfall runoff models are generally calibrated on discharge. However, this does not mean that the internal processes in the catchment are modeled correctly. Seibert and McDonnell (2002) argued that rather than being "right for the wrong reasons," process representation in hydrological modeling would be better if it were "less right, for the right reasons". If hydrological processes are better understood, models can be improved and parameters can be better estimated.

Tracers can be used to obtain a better insight in internal processes and possibly to separate hydrographs into different runoff components. Often isotopes such as deuterium (Wenninger et al., 2004), tritium or oxygen-18 (Sklash and Farvolden, 1979; Uhlenbrook and Leibundgut, 2002) are used to distinguish between event water and pre-event water. Besides these, dissolved silica and major ions (such as Cl^-, Na^+,

K^+, Ca^+ and Mg^+) are used, for a two, three or even a five component separation (Katsuyama et al., 2001; Kendall et al., 2001; Uhlenbrook and Hoeg, 2003).

A disadvantage of these tracers is that they are expensive, difficult to determine, or they do not behave conservative in the environment (e.g. ions). Another approach is to use temperature as a tracer. Kobayashi (1985), Shanley and Peters (1988) and Kobayashi et al. (1999) used temperature as a tracer, but did not determine the energy balance, which takes heating or cooling of the stream into account. Also transport processes like convection, dispersion and diffusion were not taken into account. On the other hand, temperature models exist (Brown, 1969; Webb and Zhang, 1997; Evans et al., 1998) but they generally lack knowledge on where and how much lateral inflow takes place. In the study presented here the lateral inflow is of major importance and the subject of study. Through temperature gauging we try to obtain an accurate picture of the quantity and location of lateral inflow (groundwater sources) to the stream.

We have set-up an energy balance model that determines the temperature distribution along the stream taking into account lateral inflows. We use high resolution (in space and time) temperature measurements to calibrate the temperature model and, subsequently, to estimate the amount and location of lateral inflow. It is the first time that such high resolution data are used in a coupled hydrologic and energy balance model.

2 Site description and measurements

2.1 Site description

The study site is a subcatchment of the Maisbich catchment (0.342 km^2; Fig. 1), located in central Luxemburg; latitude 49°53′ N and longitude 6°02′ E. The catchment is part of the Alzette catchment. The subcatchment is the eastern branch of the Maisbich catchment with elevations ranging from 296 to 494 m.

The bedrock consists of schist covered with a soil layer. The upper part of the wa-

tershed is mainly pasture and some settlements. The place where the stream begins is a swampy area. It is surrounded by vegetation and the landscape shows a dip. Here water from the upper part exfiltrates at different spots. Colluvial sediments are found on the surface.

Just downstream of this point a V-notch (Q4) has been installed. Further downstream the schist comes to the surface. Both sides have steep forested slopes. At four places groundwater sources are found. It is assumed that also diffuse exfiltration and infiltration take place.

The downstream boundary of the watershed is formed by a V-notch (Q3) located at the confluence with a tributary. The total length of the stretch is 580 m. During the observation period the discharge was more or less constant (1.2 l s^{-1} at Q3). Precipitation was negligible during the experiment.

2.2 Measurements

The downstream discharge has been measured at Q3 at 10 min intervals. At Q4 hand measurements were done at 2 May 2006 and 3 May 2006. The precipitation is measured by a tipping bucket recording rain gauge (TB in Fig. 1). The water temperature has been measured with a DTS (Distributed Temperature Sensing) fiber optic cable using the Sensornet system (Sentinel DTS-LR, London, England). It measures the temperature with a precision of 0.01°C and a spatial resolution of 0.5 m. Every two minutes a longitudinal temperature profile is stored. For a detailed description see Selker et al. (2006a).

Air temperature and relative humidity have been measured at Ettelbruck (ca. 7 km from the catchment) by the ASTA (Administration des services techniques de l'Agriculture, Luxembourg) at 10 min interval. As no reliable wind velocities are measured a wind velocity of 0.1 m s^{-1} is considered for the whole period. No wind was noticed in the field and the brook is sheltered by vegetation, which makes this assumption acceptable. Measured solar radiation (by satellite) from LandSAF (Land Surface Analysis Satellite Applications Facility; http://landsaf.meteo.pt) has been used for the

temperature model.

3 Methods

3.1 Model description

The temperature model makes use of a system of well mixed reservoirs. To minimize the numerical dispersion the Van Leer limiter (Van Leer, 1974) is used. The limiter estimates the stream temperature at the downstream border of each section in a non-linear way. In this way nummerical dispersion is minimized. For each section, the net energy is added. Diffusion and dispersion are assumed to be negligible within the accuracy of the model. The mass and energy balance for temperature transport are

$$\frac{\partial A}{\partial t} + \frac{\partial Q}{\partial x} = q_L \tag{1}$$

$$\frac{\partial (AT)}{\partial t} + \frac{\partial (QT)}{\partial x} = q_L T_L + R \tag{2}$$

$$R = \frac{B\Phi_{\text{total}}}{\rho_w c_w} \tag{3}$$

In finite volumes Eqs. (1) and (2) become

$$\frac{\mathrm{d}V}{\mathrm{d}t} = Q_{\text{in}} - Q_{\text{out}} + Q_L \tag{4}$$

$$\frac{\mathrm{d}(VT)}{\mathrm{d}t} = Q_{\text{in}} T_{\text{in}} - Q_{\text{out}}(T + \Delta T) + Q_L T_L + \frac{RV}{A} \tag{5}$$

Combining Eqs. (4) and (5) give

$$\frac{\mathrm{d}T}{\mathrm{d}t} = \frac{Q_{\text{in}}(T_{\text{in}} - T)}{V} - \frac{Q_{\text{out}}\Delta T}{V} + \frac{Q_L(T_L - T)}{V} + \frac{R}{A} \tag{6}$$

To reduce the consistency error in the finite difference scheme, Eq. (6) is written as:

$$\frac{dT}{dt} = \frac{Q_{in}(T_{up} - T)}{V} + \frac{Q_{in}\Delta T_{up} - Q_{out}\Delta T}{V}(1 - C) + \frac{Q_L(T_L - T)}{V} + \frac{R}{A} \quad (7)$$

where dT/dt is the change of water temperature in the section over time [°C s^{-1}], q_L is the lateral inflow per unit width [m^2 s^{-1}] and Q and T are the discharge [m^3 s^{-1}] and the water temperature [°C]. The subscripts $_{in}$, $_{out}$ and $_L$ are incoming, outgoing and lateral inflow, respectively. T is the water temperature in the center of the section, ΔT is a measure for the temperature gradient between the current and the downstream section, determined by the Van Leer limiter. T_{up} is the temperature of the upstream section, ΔT_{up} is a measure for the temperature gradient between the current section and the upstream section and C is the Courant number. V, A and B are the volume [m^3], the cross section [m^2] and the width [m] of the section. R is the sink/source term (Boderie and Dardengo, 2003[1]) where Φ_{total} is the sum of all the energy fluxes per unit area [W m^{-2}], ρ_w is the density [kg m^{-3}] of water and c_w is the specific heat capacity [J kg^{-1}°C^{-1}] of water.

3.2 Energy balance

The model takes the following energy fluxes into account: Solar radiation (including shading effects) (Φ_{solar}), longwave radiation ($\Phi_{longwave}$), streambed conduction ($\Phi_{conduction}$), latent heat ($\Phi_{evaporation}$) and sensible heat ($\Phi_{sensible\_heat}$). In Fig. 2 these processes are schematized.

Solar radiation

Solar radiation consists of direct radiation and diffuse radiation. Shadows influence the direct beam radiation, thus is important to know. Therefore critical shadow angles

[1]Boderie, P. and Dardengo, L.: Warmtelozing in oppervlaktewater en uitwisseling met de atmosfeer, Report Q3315, WL|Delft Hydraulics, 2003.

have been calculated for each grid cell. Partial shading due to vegetation is also taken into account. The diffuse radiation is not influenced by shadows. The solar radiation is computed as:

$$\Phi_{solar} = (1 - D_f)(\Phi_{direct} + \Phi_{diffuse}) \quad (8)$$

$$\Phi_{direct} = C_s(1 - D_{diffuse})\Phi_{Landsaf} \quad (9)$$

$$\Phi_{diffuse} = D_{diffuse}\Phi_{Landsaf} \quad (10)$$

where Φ_{direct} is the direct solar radiation compensated for shadow effects (factor C_s [−]). $\Phi_{Landsaf}$ is the solar radiation measured by the LandSAF satellite. D_f is the fraction [−] of solar radiation which reaches (warms up) the stream bed (and which is not used for warming up the water directly). $\Phi_{diffuse}$ is the diffuse solar radiation, and $D_{diffuse}$ is the fraction [−] of solar energy which is diffuse.

The factor C_s is zero when the stream lies completely in the shadow, and it is 1 when the stream lies completely in the sun. Due to vegetation this factor can be between zero and one. The critical topographic angle is calculated in three directions (east, south and west) while the critical land cover angles are calculated in seven directions (northeast, north, southeast, south, southwest, west and northwest). TTools, which is developed by Boyd and Kasper (2003)[2] as an Arcview GIS extension is used to calculate this.

Longwave radiation

Longwave radiation includes the atmospheric, back radiation (radiation flux emitted from the water column) and land cover longwave radiation. They are all calculated using the Stefan-Boltzman law.

[2]Boyd, M. and Kasper, B.: Analytical methods for dynamic open channel heat and mass transfer: methodology for the Heat Source Model Version 7.0, Watershed Sciences Inc., Portland, OR, USA, found at: http://www.heatsource.info/Heat_Source_v_7.0.pdf, 2003.

Atmospheric longwave radiation is the longwave radiation the water receives from the atmosphere. It is computed as (Boderie and Dardengo, 2003):

$$\Phi_{\text{atmospheric}} = 0.96\varepsilon_{\text{atm}}\sigma_{sb}(T_{\text{air}} + 273.2)^4 \quad (11)$$

$$\varepsilon_{\text{atm}} = 1.1B_c + a_1\sqrt{e_a} \quad (12)$$

$$e_s = 6.1275e^{\left(\frac{17.27T_{\text{air}}}{237.3+T_{\text{air}}}\right)} \quad (13)$$

$$e_a = \frac{H}{100\%}e_s \quad (14)$$

where T_{air} is the air temperature [°C], ε_{atm} is the emissivity of the atmosphere [–] , a_1 is an empirical constant [$(\text{hPa})^{-0.5}$] and σ_{sb} is the Stefan-Boltzman constant [$\text{W m}^{-2}\,°\text{C}^{-4}$]. H is the relative humidity [–], e_a is the actual vapour pressure [hPa], e_s is the saturation vapour pressure [hPa] and B_c is the "Brunt" coefficient [–], which is a function of air temperature and the ratio of measured solar radiation and calculated clear sky radiation (Boderie and Dardengo, 2003).

Back radiation is the energy flux emitted from the water column. It is computed as (Boyd and Kasper, 2003):

$$\Phi_{\text{back\_radiation}} = -0.96\sigma_{sb}(T + 273.2)^4 \quad (15)$$

Land cover longwave radiation is the longwave radiation received from the land cover. If vegetation is denser more radiation is emitted to the stream. This is expressed in the "view to sky" coefficient. The land cover longwave radiation is computed as (Boyd and Kasper, 2003):

$$\Phi_{\text{land\_cover}} = 0.96(1 - \theta_{\text{VTS}})0.96\sigma_{sb}(T_{\text{air}} + 273.2)^4 \quad (16)$$

where θ_{VTS} is the "view to sky" coefficient [–].

Streambed conduction

Heat energy transfer between the water and the riverbed is called streambed conduction. It is driven by thermal differences between the water and the substrate layer. The substrate layer is presented as a layer which is also influenced by energy fluxes. It is a layer between the water and the deeper alluvium. The latter is assumed to have a constant temperature. It is computed as (Boyd and Kasper, 2003):

$$\Phi_{\text{conduction}} = -K_{\text{soil}} \frac{T - T_{\text{soil}}}{d_{\text{soil}}} \tag{17}$$

$$T_{\text{soil}}^{t+1} = T_{\text{soil}}^{t} + \Delta T_{\text{soil}} \tag{18}$$

$$\Delta T_{\text{soil}} = \Phi_{\text{net}} \frac{\Delta t}{d_{\text{soil}} \rho_{\text{soil}} c_{\text{soil}}} \tag{19}$$

$$\Phi_{\text{net}} = \left(\Phi_{\text{solar}} \frac{Df}{1 - Df} - \Phi_{\text{conduction}} + \Phi_{\text{conduction}}^{\text{alluvium}} \right) \tag{20}$$

$$\Phi_{\text{conduction}}^{\text{alluvium}} = -K_{\text{soil}} \frac{T_{\text{soil}} - T_{\text{alluvium}}}{d_{\text{soil}}} \tag{21}$$

$$K_{\text{soil}} = K_{\text{sed}} (1 - \eta) + K_w \eta \tag{22}$$

$$\rho_{\text{soil}} = \rho_{\text{sed}} (1 - \eta) + \rho_w \eta \tag{23}$$

$$c_{\text{soil}} = c_{\text{sed}} (1 - \eta) + c_w \eta \tag{24}$$

where K_{soil} is the volumetric weighted thermal conductivity [$\text{J m}^{-1}\,\text{s}^{-1}\,^{\circ}\text{C}^{-1}$], T_{soil}, ρ_{soil}, d_{soil} and c_{soil} are the temperature, density, depth and specific heat capacity of the substrate layer. K_{sed} and K_w are the thermal conductivity [$\text{J m}^{-1}\,\text{s}^{-1}\,^{\circ}\text{C}^{-1}$] of the sediment and the water. ρ_{sed} and c_{sed} are the density and the specific heat capacity of the substrate. T_{alluvium} is the temperature of the deeper alluvium, η is the porosity [–] of the substrate layer and Δt is the time step [s].

Latent heat flux

Latent heat is the energy used for evaporation. It is computed using the Penman equation for open water (Monteith, 1981):

$$\Phi_{\text{evaporation}} = -\rho_w L_e E \tag{25}$$

$$L_e = 1000(2501.4 + T) \tag{26}$$

$$E = \frac{s\Phi_r}{\rho_w L_e (s+\gamma)} + \frac{c_{\text{air}}\rho_{\text{air}}(e_s - e_a)}{\rho_w L_e r_a (s+\gamma)} \tag{27}$$

$$s = \frac{4100 e_s}{(237 + T_{\text{air}})^2} \tag{28}$$

$$r_a = \frac{245}{0.54 v_{\text{wind}} + 0.5} \tag{29}$$

where L_e is the latent heat of vaporation [J kg^{-1}], E is the Penman open water evaporation [m s^{-1}]. Φ_r is the net radiation [W m^{-2}], which is the sum of the solar radiation and longwave radiation. s is the slope of the saturated vapour pressure curve at a given air temperature [hPa °C^{-1}], γ is the psychrometric constant [hPa °C^{-1}], r_a is the aerodynamic resistance [s m^{-1}] and v_{wind} is the wind speed [m s^{-1}]. c_{air} and ρ_{air} are the specific heat capacity and the density of air.

Sensible heat flux

The sensible heat flux is the heat exchange between the water and the air, which is driven by thermal differences. It is computed as (Boyd and Kasper, 2003):

$$\Phi_{\text{sensible\_heat}} = B_r \Phi_{\text{evaporation}} \tag{30}$$

$$B_r = 6.1 \cdot 10^{-4} P_A \frac{T - T_{\text{air}}}{e_s^w - e_a^w} \tag{31}$$

$$e_s^w = 6.1275 e^{\left(\frac{17.27T}{237.3+T}\right)} \tag{32}$$

$$e_a^w = \frac{H}{100\%} e_s^w \tag{33}$$

$$P_A = 1013 - 0.1055z \tag{34}$$

where B_r is Bowen Ratio [–], e_s^w and e_a^w are the saturated and actual vapour pressure [hPa] using the stream temperature, P_A is the adiabatic atmospheric pressure [hPa] and z is the elevation height [m] of the measured humidity and air temperature.

3.3 Determination of lateral inflow

To derive the lateral inflow of single sources the mass and heat conservation equations are used (Kobayashi, 1985):

$$Q_d = Q_u + Q_L \tag{35}$$

$$T_d Q_d = T_u Q_u + T_L Q_L \tag{36}$$

where Q is discharge [$m^3 s^{-1}$], T is the water temperature and the subscripts $_d$, $_u$ and $_L$ are downstream, upstream and lateral inflow, respectively. The ratio between Q_L and Q_d can be derived by solving Eqs. (35) and (36):

$$\frac{Q_L}{Q_d} = \frac{T_d - T_u}{T_L - T_u} \tag{37}$$

where T_L is still unknown. There are two ways to define the temperature of the lateral inflow:

1. At the moment when no jump in the longitudinal profile can be seen, the temperature of the source is the same as the measured upstream and downstream temperature. Selker et al. (2006b) have used this method for the same dataset.

2. T_L can be derived from two profiles at different times. The assumptions are that Q_L/Q_d and T_L are constant over the time between the two series. Using Eq. (37) for two profiles will result in

$$\frac{T_{d_1} - T_{u_1}}{T_L - T_{u_1}} = \frac{T_{d_2} - T_{u_2}}{T_L - T_{u_2}} \tag{38}$$

and hence

$$T_L = \frac{T_{d_2}T_{u_1} - T_{u_2}T_{d_1}}{T_{d_2} - T_{u_2} - T_{d_1} + T_{u_1}} \tag{39}$$

where the subscripts $_1$ and $_2$ relate to the two profiles. Q_L/Q_d can also be calculated directly from two profiles using Eq. (37)

$$\frac{Q_L}{Q_d} = \frac{T_{d_2} - T_{u_2} - T_{d_1} + T_{u_1}}{T_{u_1} - T_{u_2}} \tag{40}$$

Equation (40) makes it easier to determine the accuracy, which is necessary to know because in this method large errors can occur in the derivation of Q_L/Q_d, due the propagation of errors in the process of subtracting. The relative error r is given by:

$$r^2_{\left(\frac{Q_L}{Q_d}\right)} = \frac{\sigma^2_{\left(T_{d_2}\right)} + \sigma^2_{\left(T_{u_1}\right)} + \sigma^2_{\left(T_{u_2}\right)} + \sigma^2_{\left(T_{d_1}\right)}}{\left(T_{d_2} - T_{d_1} + T_{u_1} - T_{u_2}\right)^2} + \frac{\sigma^2_{\left(T_{u_1}\right)} + \sigma^2_{\left(T_{u_2}\right)}}{\left(T_{u_1} - T_{u_2}\right)^2} \tag{41}$$

where σ is the standard deviation of the measured temperature. Several combinations of two different profiles are taken to do this calculation (from 0.5 h until 16 h between the two profiles). If two profiles are close or if the jump in one profile is not significant large errors can occur. As a result we have used all combinations of profiles within a period of 16 h that had a smaller relative error than 10%, and subsequently taken the average of the remaining set. In addition the standard deviation and the coefficients of variance ($CV = \sigma/\text{average}$) have been calculated to define the accuracy of T_L and Q_L/Q_d.

3.4 Assumptions

In this study several assumptions have been made. Regarding the lateral inflow determination in Eqs. (39) and (40) the assumption is made that over the time interval between the two profiles T_L and Q_L/Q_d are constant. The small coefficients of variance of T_L and Q_L/Q_d make this assumption valid (Table 1).

Regarding the temperature model, the assumption have been made that the discharge is constant over time and is only changing when a groundwater source is coming in. This implies constant stream velocity and constant volume of each reservoir over time. This is a valid assumption since the observed discharge showed only a small variation around the average.

Other assumptions are that no diffuse sources enter the stream and there is no loss of water. The temperature of the alluvium is equal to groundwater ($T_{\text{alluvium}} \approx T_L$), the "view to sky" coefficient is constant along the stream, no diffusion and dispersion take place and observed air temperature and relative humidity of a nearby station are representative for the study site.

4 Results

Over the stream reach four sources can be distinguished (Fig. 3). We also see large fluctuations in temperature (in time as well as in space). Small short peaks are measured at places were the cable was out of the water (e.g. at a small water fall at 404 m). At 06:00 a.m. the first two sources cause warming up of the stream while later in the day temperature drops occur at these places.

In Table 1 the calculated temperatures and relative contributions of each source are given. The difference between the temperature of a source using the two different methods are within 0.15°C for the first three sources and 0.26°C for source 4 which is only 3% of T_L. For source 4 this is equal to the standard deviation of T_L (Table 1) while for the first three sources this is even smaller than the standard deviation.

The differences between T_L and T_L^* may occur because T_L^* is always calculated in relative cold circumstances while the other method returns into daily average temperature which might be slightly different.

For all further calculations T_L and Q_L/Q_d have been determined by Eqs. (39) and (40). With a discharge of $1.2\,\mathrm{l\,s^{-1}}$ at Q3 the absolute contributions of the four sources are: 0.33, 0.24, 0.15 and $0.28\,\mathrm{l\,s^{-1}}$, respectively.

In the energy balance a lot of data are needed. Most of these are time or place dependent (or both). The parameters and constants which are time and place independent are listed in Table 2. The constants D_f, D_{diffuse}, θ_{VTS}, and K_{sed} have been calibrated of which D_f and D_{diffuse} are the most sensitive. The other constants have been taken from literature.

The simulation period is from 23 April 2006 12:00 till 30 April 2006 00:00. The upper plot in Fig. 4 shows the calculated and measured temperature just upstream of source 1 (at 110 m), while the bottom one shows the results just downstream of this source. The source has a clear influence on the daily maxima. The daily minima remain more or less the same. The source has less influence on this because the stream temperature is closer to the temperature of the source.

HESSD
4, 125–149, 2007

EGU

Solar radiation is the main flux responsible for the daily variation (Fig. 5). Conduction has a dimming effect on the water temperature. During the day it functions as an energy sink while during the night it is a source of energy. The longwave atmospheric radiation and the back radiation are both large, but they are rather constant over time. Hence they do not cause large changes in temperature. Latent heat is significant when it is sunny, while it is small during the night and when it is cloudy.

5 Discussion

In the model the peaks are modeled well, especially the first 3 days. A structural problem is that in the model the water cools down too fast. This can be due to different reasons. The conduction with the riverbed is an important flux in the cooling down period. Because during the day the riverbed warms up and gives its energy back to the water when it is getting colder. Three out of the four calibration constants influence this flux. By measuring these constants this flux will become closer to reality and uncertainty due to calibration will be reduced.

Also shading effects can be a source of errors. Because the stream is so small, small errors in height of trees and bushes can have big influences.

Another flux which may have a significant influence is the land cover longwave radiation. In this study the "view to sky" coefficient (θ_{VTS}) is taken constant along the stream. In reality this is not the case. By making this coefficient smaller the radiation will become larger. With the calibration a "best average" is taken for this constant. This influences the temperature more in space than in time.

The latent heat flux uses the solar and longwave radiation as input. Because latent heat is a negative flux it reduces errors made in the solar and longwave radiation. The inaccurate chosen wind velocity is point of discussion and should be determined better. During the observation period hardly any wind has been noticed, which makes the influence of wind on evaporation small compared to the total evaporation. We recognize that this will not be the case in more windy circumstances.

Losses of water (due to evaporation and infiltration) and diffuse sources can also be sources of errors, since they are not taken into account in the model. Using data of 2 May 2006 a net loss of 19% is calculated (as the difference between Q3 minus all sources and Q4). Further research has to be done to quantify these losses. To do so the volumes can be better quantified.

Although the temperature model can be improved, the study shows a good application of the DTS technique. It gives high resolution data and is an interesting new technique to make the complex mechanisms of surface water groundwater interactions of small scale catchments visible.

6 Conclusions

Due to the DTS measuring technique high resolution data are available for model input (lateral inflow) and calibration. Even though the temperature model has some simplification (e.g. constant discharge, no diffuse losses or sources) it shows good results: Results which are not verifiable without this technique. With classical measuring techniques it is not possible to have time series every 0.5 m along the stream.

Acknowledgements. This research has been funded partly by the Delft Cluster project Veiligheid tegen overstromingen: CT04.30. The authors would like to thank the municipality of Ettelbruck for their cooperation and J. Friesen, J. Liebe, M. Poolman, M. Baptist, R. Schilperoort, E. Tromp, and B. Baartman for their support in the field.

References

Brown, G. W.: Predicting temperature of small streams, Water Resour. Res., 5, 68–75, 1969. 127

Evans, E. C., McGregor, G. R., and Petts, G. E.: River energy budgets with special reference to river bed processes, Hydrol. Processes, 12, 575–595, 1998. 127

Katsuyama, M., Ohte, N., and Kobashi, S.: A three-component end-member analysis of streamwater hydrochemistry in a small Japanese forested headwater catchment, Hydrol. Processes, 15, 249–260, 2001. 127

Kendall, C., McDonnell, J. J., and Gu, W.: A look inside "black box" hydrograph separation models: a study at the Hydrohill catchment, Hydrol. Processes, 15, 1877–1902, 2001. 127

Kobayashi, D.: Separation of the snowmelt hydrograph by stream temperatures, J. Hydrol., 76, 155–165, 1985. 127, 135

Kobayashi, D., Ishii, Y., and Kodama, Y.: Stream temperature, specific conductance and runoff processes in mountain watersheds, Hydrol. Processes, 13, 865–876, 1999. 127

Monteith, J. L.: Evaporation and surface temperature, Quart. J. R. Meteorol. Soc., 107, 1–27, 1981. 134

Seibert, J. and McDonnell, J. J.: On the dialog between experimentalist and modeler in catchment hydrology: use of soft data for multi-criteria model calibration, Water Resour. Res., 38, 1231–1241, 2002. 126

Selker, J. S., Thévenaz, L., Huwald, H., Mallet, A., Luxemburg, W., Van de Giesen, N., Stejskal, M., Zeman, J., Westhoff, M., and Parlange, M. B.: Distributed fiber optic temperature sensing for hydrologic systems, Water Resour. Res., 42, W12202, doi:10.1029/2006WR005326, 2006a. 128

Selker, J. S., Van de Giesen, N., Westhoff, M. C., Luxemburg, W., and Parlange, M.: Fiber optics opens window on stream dynamics, Geophys. Res. Lett., 33, L24401, doi:10.1029/2006GL027979, 2006b. 136, 143

Shanley, J. B. and Peters, N. E.: Preliminary observations of streamflow generation during storms in a forested Piedmont watershed using temperature as a tracer, J. Contam. Hydrol., 3, 349–365, 1988. 127

Sklash, M. G. and Farvolden, R. N.: The role of groundwater in storm runoff, J. Hydrol., 43, 45–65, 1979. 126

Uhlenbrook, S. and Hoeg, S.: Quantifying uncertainties in tracer-based hydrograph separations: a case study for two-, three- and five-component hydrograph separations in a mountainous catchment, Hydrol. Processes, 17, 431–453, 2003. 127

Uhlenbrook, S. and Leibundgut, C.: Process-oriented catchment modelling and multiple-response validation, Hydrol. Processes, 16, 423–440, 2002. 126

Van Leer, B.: Towards the ultimate conservative difference scheme II. Monotonicity and conservation combined in a second order scheme, J. Comput. Phys., 14, 361–370, 1974. 129

Webb, B. W. and Zhang, Y.: Spatial and seasonal variability in the components of the River heat budget, Hydrol. Processes, 11, 79–101, 1997. 127

Wenninger, J., Uhlenbrook, S., Tilch, N., and Leibundgut, C.: Experimental evidence of fast groundwater responses in a hillslope/floodplain area in the Black Forest Mountains, Germany, Hydrol. Processes, 18, 3305–3322, 2004. 126

Table 1. Calculated temperature and relative contributions of the four sources. Point 1 is the most upstream source and point 4 the most downstream.

inflow point	T_L^* [°C]	T_L [°C]	Q_L/Q_d [%]	$\sigma^2_{(T_L)}$ [°C]	$\sigma^2_{\left(\frac{Q_L}{Q_d}\right)}$ [%]	$CV_{(T_L)}$ [–]	$CV_{\left(\frac{Q_L}{Q_d}\right)}$ [–]
1	9.08	9.11	58.5	0.37	7.89	0.04	0.13
2	8.70	8.85	30.0	0.23	4.27	0.03	0.14
3	8.77	8.91	15.2	0.22	0.87	0.02	0.06
4	8.44	8.18	22.8	0.24	2.6	0.03	0.11

* Temperature of lateral inflow calculated when no jumps are seen. (From Selker et al., 2006b).

Table 2. Constants used in the model.

Constant	Value
D_f [–]	0.5
D_{diffuse} [–]	0.3
θ_{VTS} [–]	0.9
T_{alluvium} [°C]	9
σ_{sb} [W m^{-2} °C^{-1}]	5.67· 10^{-8}
γ [hPa °C^{-1}]	0.66
ρ_w [kg m^{-3}]	1000
ρ_{sed} [kg m^{-3}]	1600
ρ_{air} [kg m^{-3}]	1.205
c_w [J kg^{-1} °C^{-1}]	4182
c_{sed} [J kg^{-1} °C^{-1}]	2219
c_{air} [J kg^{-1} °C^{-1}]	1004
K_w [J m^{-1} s^{-1} °C^{-1}]	0.6
K_{sed} [J m^{-1} s^{-1} °C^{-1}]	10
d_{soil} [m]	0.2
z [m]	2
a_1 [(hPa)$^{-0.5}$]	0.03

HESSD
4, 125–149, 2007

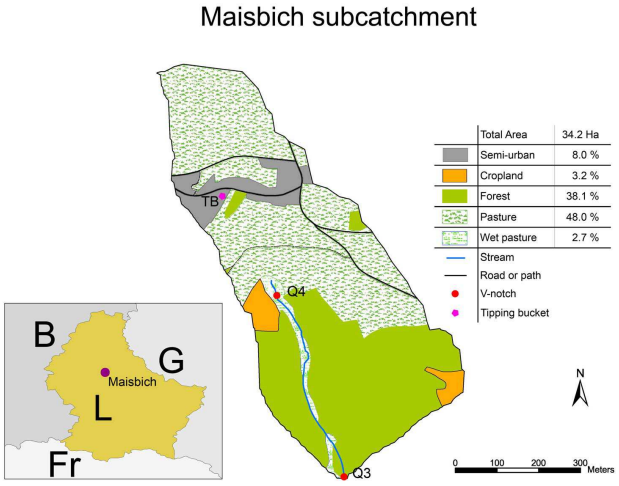

Fig. 1. Studied subcatchment of the Maisbich catchment. B=Belgium, G=Germany, Fr=France, L=Luxembourg.

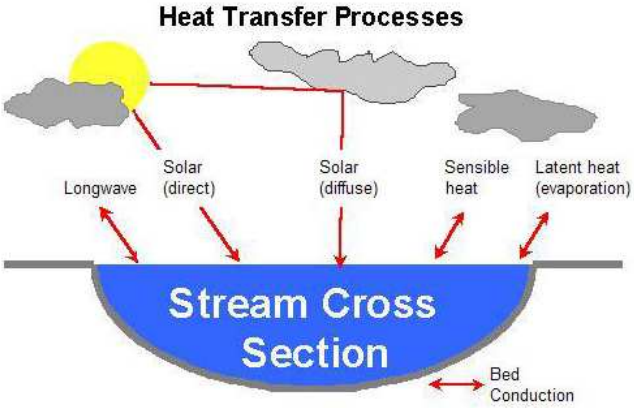

Fig. 2. Schematization of heat transfer processes (Boyd and Kasper, 2003).

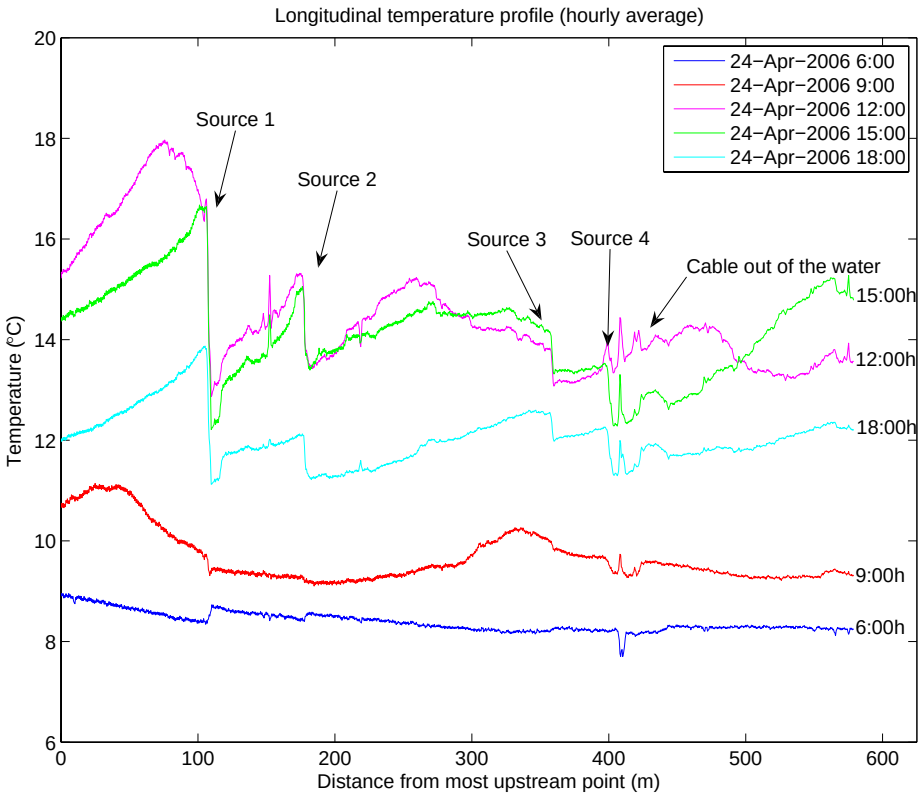

Fig. 3. Measured longitudinal temperature profile of the stream at different times during one day. Clear temperature jumps can be seen at the points of a source. Short peaks are due to the fact that the cable is out of the water for a short distance.

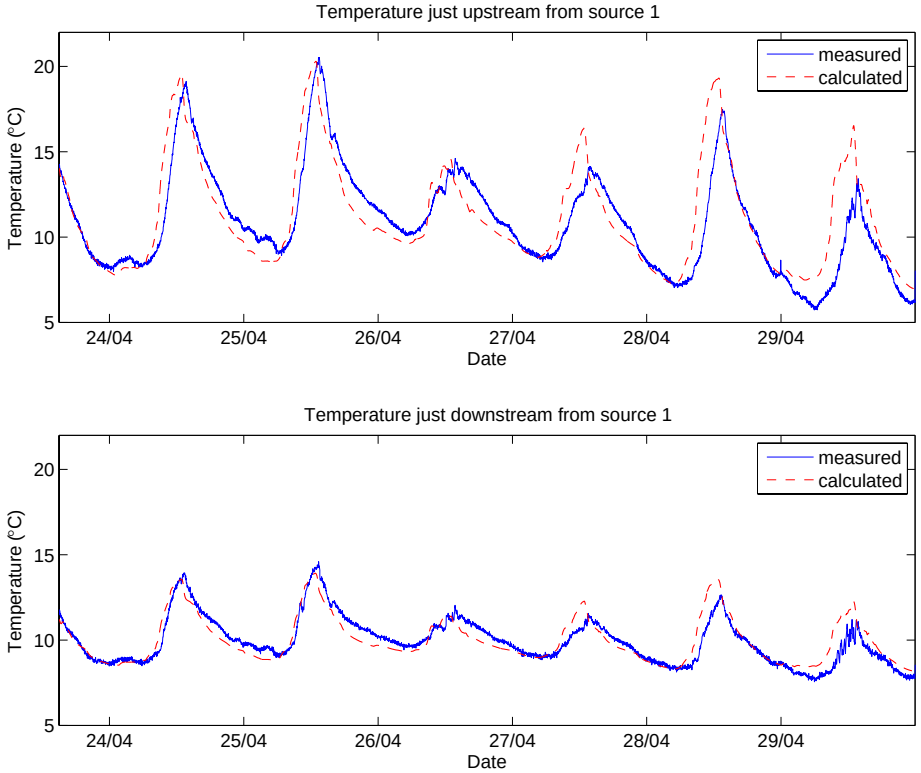

Fig. 4. Calculated and measured temperature of the investigated stream. The upper one is just upstream of source 1 and the lower one just downstream. The source is at 110 m from the most upstream point.

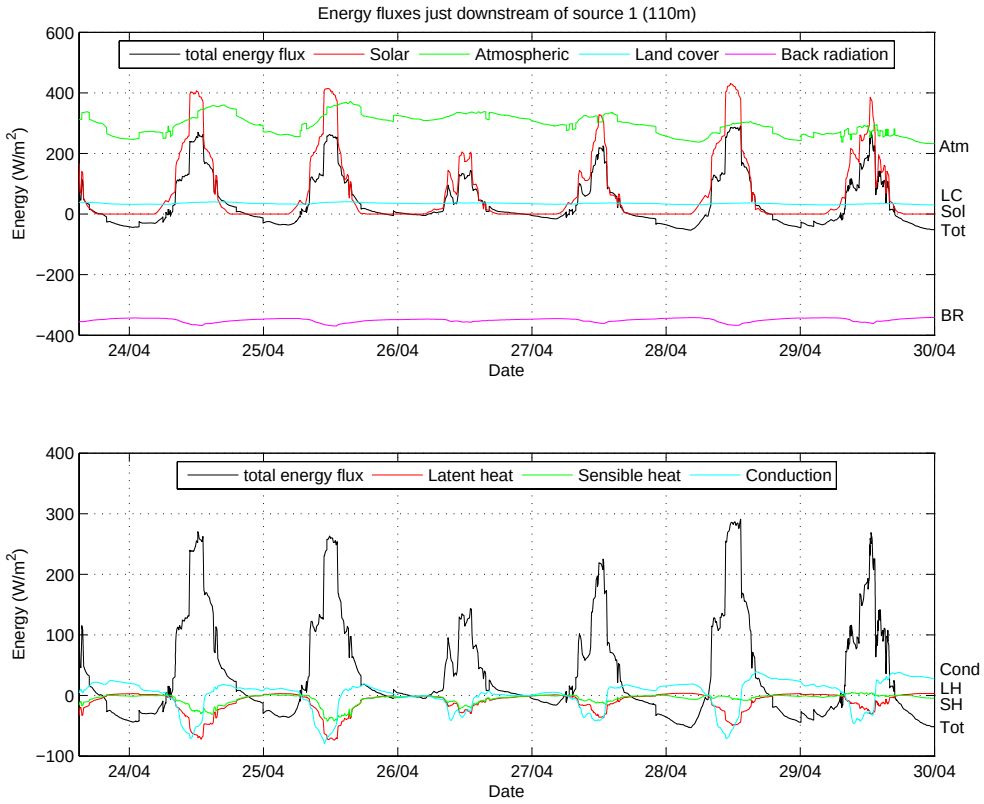

Fig. 5. Heat energy fluxes at source 1.

HESSD
4, 125–149, 2007